Speciated Atmospheric Mercury on Haze and Non-haze Days in an Inland City in China

Qianqian Hong[1,3], Zhouqing Xie[1,2,3*], Cheng Liu[1,2,3*], Feiyue Wang[4], Pinhua Xie[2,3], Hui Kang[1], Jin Xu[2], Jiancheng Wang[1], Fengcheng Wu[2], Pengzhen He[1], Fusheng Mou[2],Shidong Fan[1],Yunsheng Dong[2], Haicong Zhan[1], Xiawei Yu[1], Xiyuan Chi[1], Jianguo Liu[2]

1. School of Earth and Space Sciences, University of Science and Technology of China, Hefei, 230026, China

2. CAS Center for Excellence in Regional Atmospheric Environment& Institute of Urban Environment of CAS, Xiamen, 361021, China

3. Key Lab of Environmental Optics and Technology, Anhui Institute of Optics and Fine Mechanics, Chinese Academy of Sciences, Hefei, 230031, China

4. Centre for Earth Observation Science, and Department of Environment and Geography, University of Manitoba, Winnipeg, MB R3T 2N2, Canada

Correspondence author:

zqxie@ustc.edu.cn (Z.Q.X.); chliu81@ustc.edu.cn (C.L.)

Abstract. Long-term continuous measurements of speciated atmospheric mercury were conducted from July 2013 to June 2014 at Hefei, a mid-latitude inland city in east central China that experiences frequent haze pollution. The mean concentrations (±standard deviation) of gaseous elemental mercury (GEM), gaseous oxidized mercury (GOM) and particle-bound mercury (PBM) were 3.95 ± 1.93 ng m^{-3}, 2.49 ± 2.41 pg m^{-3} and 23.3 ± 90.8pg m^{-3}, respectively, on non-haze days, and 4.74 ±1.62 ng m^{-3}, 4.32 ± 8.36 pg m^{-3} and 60.2 ± 131.4 pg m^{-3}, respectively, on haze days. Potential source contribution function (PSCF) analysis suggested that atmospheric mercury pollution on haze days was caused primarily by local emissions, instead of via long-range transport. The poorer mixing conditions on haze days also favored the accumulation of atmospheric mercury. Compared to GEM and GOM, PBM was especially sensitive to haze pollution. The mean PBM concentration on haze days was 2.5 times that on non-haze days due to elevated concentrations of particulate matter. PBM also showed a clear seasonal trend; its concentration was the highest in autumn and winter, decreased rapidly in spring, and was the lowest in summer, following the same order in the frequency of haze days in different seasons. On both non-haze and haze days, GOM concentrations remained low at night, but increased rapidly just before sunrise, which could be due to diurnal variation in air exchange between the boundary layer and free troposphere. However, non-haze and haze days showed different trends in daytime GEM and GOM concentrations. On non-haze days, GEM and GOM declined synchronously through afternoon, probably due to the retreat of the free tropospheric air as the height of the atmospheric boundary layer increases. In contrast, on haze days, GOM and GEM showed opposite trends with the highest GOM and lowest GEM observed in the afternoon, suggesting the occurrence of

photochemical oxidation. This is supported by simple box-model calculations, which showed that oxidation of GEM to GOM does occur and that the transport of free tropospheric GOM alone is not large enough to account for the observed increase in daytime GOM. Our results further postulate that NO_2 aggregation with the HgOH intermediate may be a potential mechanism for the enhanced production of GOM during daytime.

1. Introduction

Mercury (Hg) is an environmental pollutant that has received much global attention because of its toxicity and bioaccumulation in theaquatic ecosystems. The most important transport pathway of mercury is via the atmosphere(Schroeder and Munthe, 1998;Lindqvist and Rodhe, 1985). Operationally,atmospheric mercury is commonly differentiated into threeforms:gaseous elemental mercury (GEM), gaseous oxidized mercury (GOM) and particle-bound mercury (PBM). The sum of these three atmospheric speciated mercury is defined as total atmospheric mercury (TAM=GEM+GOM+PBM), and the sum of GEM and GOM is known as total gaseous mercury (TGM=GEM+GOM)(Gustin and Jaffe, 2010;Gustin et al., 2015). Globally GEM is the dominant form of atmospheric mercury, accounting for over 95% of the total. GEM is stable in the troposphere with a long residence time (0.5–2 yr) and can be transported at the regional to global scale(Schroeder and Munthe, 1998;Lindberg et al., 2007). GEM can be photochemically oxidized to GOM, which can be converted to PBM upon adsorption on aerosol surfaces. Different from GEM, GOM and PBM can be readily removed form the air by wet and dry depositionas a result oftheir high surface affinity and water solubility (Lindqvist and Rodhe, 1985).

Thus, chemical transformation between GEM, GOM and PBM will directly influence the atmospheric lifetime of mercury.

As a result of rapid industrial development and economic growth in recent decades, China hasbecome one of the major contributors to anthropogenic mercury emissions to the environment(Wu et al., 2006;Pacyna et al., 2006;Pacyna et al., 2010;Zhang et al., 2015b). Atmospheric mercury emissions from anthropogenic sources in China have been estimated to be in the range of 500-700 tons/yr, accounting for 25-30% of the total global anthropogenic mercury emissions(Streets et al., 2005;Wu et al., 2006). Studies of atmospheric mercury in China are therefore critical to the understanding of mercury cycling at both regional and global scales. Long-term observation of atmospheric mercury has been conducted in numerous urban and remote areas in China. TGM concentrations in urban and industrial areas were observed to be in the range of 2.7–35 ng m^{-3}, higher than the values reported for North America and Europe, and for the adjacent Asian countries such as Korea and Japan (Weigelt et al., 2013;Fang et al., 2009;Marumoto et al., 2015). TGM and PBM concentrations in remote areas of China were also found to be higher than those observed in North America and Europe(Fu et al., 2008a;Fu et al., 2008b;Fu et al., 2012;Liu et al., 2010).

In recent years, haze pollution has become a major concern in China due to its impacts on visibility, air quality, and climate. It is well known that haze formation is mainly dependent on the atmospheric relative humidity (RH) and the concentration of airborne particles(Chen et al., 2003;Sun et al., 2013). Most studies on haze have focused on the measurements of airborne particulate matter; few examined the influence of haze on the chemistry of atmospheric mercury, especially PBM. Here we

report a one-year real-time measurement of speciated atmospheric mercury in Hefei, an inland city of China, which experiences frequent haze events. The comparision of atmospheric mercury in haze days and non-haze days allows us to examine the formation and deposition mechanisms of mercury, as well as their temporal variations.

2. Methods

2.1 Study site

Hefei (31°52′ N, 117°17′ E)is the capital of Anhui Province in east central China, between the Changjiang (Yangtze River) and the Huaihe (HuaiRiver). The region is under a humid subtropical climate with four distinct seasons: summer (June-August), autumn (September-November), winter (December-February), and spring (March-May). The prevailing wind is southeasterly in summer and northwesterly in winter. Like many Chinese cities, Hefei has experienced rapid growth in the past 20 years, with a present-day total permanent population of about 7.7 million. The city has also been witnessing an increasing frequency in haze pollution, especially in winter months.

The monitoring site was located on the Science Island, a small peninsula on the Dongpu Reservoir in the northwestern outskirts of Hefei (Fig. 1). The sampling and analytical instruments were installed 1.5 m above the rooftop (~ 20 m above the ground) of the main building of Anhui Institute of Optics and Fine Mechanics. Further information about the monitoring site can be found in a previous study (Hu et al., 2014). We chose this area as the monitoring site because it is not adjacent to any direct pollution sources such as power plants, iron and steel works.

2.2 Measurements of speciated atmospheric mercury

From July 2013 to June 2014, simultaneous measurements of GEM, GOM and PBM were carried out by an automated Tekran^{TM}mercury speciation system. The system consisted of a Model 2537B mercury analyzer combined with a Model 1130 GOM unit and a Model 1135 PBM unit. The system was configured to measure GEM every 5 min., and GOM and PBM every 2 h.

The details about the Tekran-based mercury speciation system can be found in Landis et al. (2002). In general, the automated measurement process can be summarized as sample collection, thermal desorption and determination. During the collection period, ambient air is drawn to the system at a typical flow rate of 10 L/min. GOM and PBM in the air are captured by a KCl-coated quartz annular denuder in the 1130 unit and a quartz filter in the 1135 unit, respectively, whereas GEM would pass through the denuder and filter and be quantified on the 2537B analyzer by cold-vapor atomic fluorescence spectroscopy (CVAFS). After an hour of sampling, the 1135 quartz filter and the 1130 denuder would be switched to the thermal decomposition mode at 800°C and 500°C, respectively, with the resulting Hg^0quantified by the 2537B unit in the next hour, while the 1135 and 1130 components are flushed with zero-mercury gas for the next sampling.

The instrument maintenance followed typical protocols used in similar studies(Landis et al., 2002;Hu et al., 2014). The quartz annular denuder was recoated every two weeks, the quartz filter was replaced once a month, and the Teflon filter (pore size 0.2 μm) in the sample inlet was changed every two weeks. Automated recalibration of the Tekran 2537B was performed every 25h using an internal mercury permeation source.No calibration standards were available for GOM and PBM, but

the 1σ precision for GOM and PBM was about 15 % (Landis et al., 2002). The detection limit in ambient air is about 0.5 ng $m^{-3}$for GEM (or TGM) at a resolution of 5 min, and 1 pg $m^{-3}$for GOM and PBM at a resolution of 2h (Gustin et al., 2015). Although the Tekran-based mercury speciation technique has been widely used around the world, recent studies have shown that the technique does not efficiently collect all GOM and thus may substantially underestimate the concentration of reactive mercury (Huang et al., 2013;Gustin et al., 2013). Therefore, the GOM values reported in this study should be considered as the lower limit of GOM in the air(Wang et al., 2014).

2.3 Ancillary data

Standard meteorological measurements including air temperature, pressure, RH, wind direction and speed were observed witha 5-min resolution. CO was measured by an automated infrared carbon monoxide analyzer (Model EC9830T, Ecotech Inc., Australia), with a detction limitof 40 ppbv. $O_3$was measured every 5 min by an ozone analyzer (Model EC9810B, Ecotech Inc., Australia); its detection limit and accuracy were 0.5 ppbv and 1 ppbv, respectively.NO_2 was measured by a Multi axis differential optical absorption spectroscopy (MAX-DOAS) instrument. The collected spectra were analyzed using the QDOAS spectralfitting software suite developed at BIRA-IASB (http://uv-vis.aeronomie.be/software/QDOAS/).$PM_{2.5}$ (particulate matter of less than 2.5 μm in diameter) data were collected from the China air quality online analysis platform (http://www.aqistudy.cn/historydata/index.php).

2.4 Potential Sources Contribution Function (PSCF) analysis

To identify possible influence of long-range transport on the distribution of atmospheric mercury in Hefei, we calculated backward trajectories of air masses using the HYSPLIT (Hybrid Single-particle Lagrangian Integrated Trajectory) model with the Global Data Assimilation System (GDAS 1°) developed by the National Oceanic and Atmospheric Administration (NOAA) (*http://www.ready.noaa.gov*)(Draxler and Hess, 1998). Considering atmospheric pollutants are mainly concentrated in low altitudes during heavy pollution days, the trajectory arrival heights were set at 500m to represent the boundary layer where atmospheric pollutants were well mixed.In this study,3-day back-trajectories were generated hourly by the TrajStat software, which employs HYSPLIT for trajectory calculation(Wang et al., 2009).

The contributions of other source regions to the atmospheric mercury at Hefei were identified by the Potential Sources Contribution Function (PSCF) analysis with TrajStat. PSCF analysis has been shown to be useful in spatially identifying emission sources for pollutants with a long lifetime such as elemental mercury and CO (Xu and Akhtar, 2010). The study domain is divided into grid cells, and the PSCF value for each cell was calculated by counting the trajectory segment endpoints that terminate within the cell. The PSCF value for the ij_{th} cell is defined as:

$$PSCF_{ij} = \frac{M_{ij}}{N_{ij}} W_{ij} \quad (2)$$

where N_{ij} is the number of endpoints that fall in the ij_{th} cell, and M_{ij} is the number of endpoints in the the same cell that has a GEM concentration higher than an arbitrarily set criterion; in this study the criterion was set to be 4 ng m^{-3}which is the mean GEM concentration during the entire study period.W_{ij} is an arbitrary weight function introduced to reduce the effect of small values of N_{ij} to better reflect the uncertainty in

the values for these cells (Polissar et al., 2001).The weight function reduces the PSCF values when the total number of endpoints in a particular cell is less than 3 times the average value of the end points per cell:

$$W_{ij} = \begin{cases} 1.0 & N_{ij} \geq 3N_{ave} \\ 0.70 & 3N_{ave} > N_{ij} \geq 1.5N_{ave} \\ 0.40 & 1.5N_{ave} > N_{ij} \geq N_{ave} \\ 0.20 & N_{ave} > N_{ij} \end{cases} \quad (3)$$

3. Results

We intended to continuously monitor speciated atmospheric mercury concentrations over the course of a year; however, interruptions were inevitable due to instrument maintenance, which resulted in loss of data for the following four periods: (1) 25 September to 9 October 2013; (2) 5 – 14 November 2013; (3) 9 – 25 February 2014; and (4) 1 – 14 April 2014. The rest of the data were grouped into haze days and non-haze days according to the China Meteorological Administration's haze standard (QX/T 113-2010). Haze days refer to the days when the atmospheric visibility < 10 km and RH < 80% (Duan et al., 2016), and non-haze days refer to clear days with the atmospheric visibility > 10 km. The visibility and RH information were collected from the weather history data at the Luogang Airport of Hefei (http://www.wunderground.com/).Throughout the study period of almost a year, a total of 56 days were identified to be haze days, and 253 days to be non-haze days. All the times reported herein are local time (UTC + 8 h).

3.1 Overall characteristics of speciated atmospheric mercury

The time series of GEM, GOM and PBM concentrations at the study site throughout the study period are shown in Fig. 2; their frequency distributions are

shown in Fig. S1 in the supporting information (SI).The mean (± standard deviation) GEM, GOM and PBM concentrations during the entire study period were 4.07±1.91 ng m^{-3}, 3.67±5.11 pg m^{-3}, and 30.0±100.3 pg m^{-3}, respectively (Table 1).GEM concentrations in different seasons did not differ much, with the highest in autumn (4.51±2.10 ng m^{-3}) and the lowest in spring (3.89±1.79 ng m^{-3}). GOM concentrations varied greatly, with much higher concentrations in autumn and the lowest in winter. A similar seasonal variation in the GOM concentration was observed at a remote site in Mt. Gongga of southwest China(Fu et al., 2008b). PBM showed the highest degree of seasonal variability; its concentration decreased in the following order: autumn≈ winter> spring > summer. The mean PBM concentrations in autumn and winter were about 20 times that in summer, similar to the findings from many previous studies in China(Zhang et al., 2013;Fu et al., 2011;Fu et al., 2008b;Fang et al., 2001).

Comparisons of speciated atmospheric mercury concentrations with other urban and rural areas in China and a few other countries areshown in Table 2.The mean GEM concentration at Hefei is slightly higher than those reported from many remote areas in China (Fu et al., 2008a;Fu et al., 2008b;Fu et al., 2012;Wan et al., 2009a;Wan et al., 2009b; Zhang et al., 2015a), but is much lower than those from urban areas of heavily industrial cities such as Guiyang and Changchun where large point sources of mercury exist (e.g., non-ferrous metal smelting, coal-fired power plants, and residential coal burning) (Feng et al., 2004;Fu et al., 2011;Fang et al., 2004). Although Hefei is geographically close to Shanghai, a mega urban centre in China, it is interesting to note that the TGM concentration of Shanghai is much lower than that of Hefei. This may be due to the fact that Shanghai is a coastal city that is influenced more by cleaner marine air masses (Friedli et al., 2011). Table 2 also shows that the

240 average concentration of GEM in Hefei doubles the typical values reported from the
241 urban and rural areas in Europe and North America (Liu et al., 2010;Li et al.,
242 2008;Brooks et al., 2010).
243
244 **3.2Speciated atmospheric mercury on non-haze days**
245 As shown in Table 1 and Fig.S1(in blue), the mean concentration of GEM on
246 non-haze days was 3.95 ± 1.93 ng m^{-3}. Its distribution was characterized by large
247 variations ranging from 0.2 to 23.8 ng m^{-3}, although more than half of the GEM
248 values were in the narrow range 2– 4 ng m^{-3}. The mean concentration of GOM on
249 non-haze days was 2.49 ± 2.41 pg m^{-3} with a range of 0.5– 33.5 pg m^{-3}, although
250 most of the values were in the range of 1-4 pg m^{-3}. High concentrations of GOM
251 (exceeding 10 pg m^{-3}) only accounted for 1.4% of the total data points. The mean
252 GOM concentration at Hefei on these non-haze days is much smaller than those
253 reported from other study sites in China (Table 2), but is comparable to thevalues
254 observed from many European and North American sites (Peterson et al., 2012;Cheng
255 et al., 2014;Ren et al., 2016). The mean PBM concentraion on non-haze days was
256 23.3 ± 90.8 pg m^{-3} with anexceptionally large range of 0.5-1827 pg m^{-3}; high PBM
257 concentrations (i.e., > 50 pg m^{-3}) accounted for 6.4% of the total data points. The
258 PBM concentration under the non-haze condition in Hefei is generally similar to
259 values reported from remote areas in western China, such as Mt.Gongga,
260 Mt.Waliguan and Shangri-La.
261 Diurnal variations of GEM, PBM and GOM concentrations onnon-haze days are
262 shown in Fig. 3. Both GEM and PBM concentrations exhibited similarpatterns with
263 elevated concentrationsat night. The GOM concentration remained relatively constant

at night, but increased rapidly just before sunrise and reached its peak value at ~10:00, followed by a synchronous decline with GEM through afternoon (10:00-18:00).

3.3 Speciated atmospheric mercury on haze days

Haze pollution mainly occurred in December and January at our monitoring site. The four major haze pollution periods were identified in grey in Fig.2. The mean concentrations of GEM, GOM and PBM on these haze days were 4.74 ±1.62 ng m^{-3}, 4.32 ± 8.36 pg m^{-3} and 60.2 ± 131.4 pg m^{-3}, respectively (Table 1). The frequency distributions of GEM, GOM and PBM on the haze days are shown in Fig.S1 (in gray).GEM, GOM and PBM concentrations show siginificant differences between haze and non haze days ($p<0.001$, t-test) (Fig. S2). On average, the concentration of GEM on haze days was 1.2 times that on non-haze days. Similarly, the concentration of GOM on haze days was about 1-1.7 times those on non-haze days. The largest impact of haze pollution is however on PBM, with the mean PBM concentration on haze days about 2.5 times that of non-haze days. High concentrations of GOM (exceeding 10 pg m^{-3}) and PBM concentrations (exceeding 50 pg m^{-3}) were also more frequently observed on haze days, accounting for 5.9% and 25%, respectively, of the total haze days.

As shown in Fig. 3,on haze days the GEM concentration was higher at night and lower during daytime. PBM typically peaked just before sunrise, with the lowest values occurred in the afternoon (14:00-16:00). The opposite pattern was observed for GOM, which showed higher concentrations during daytime than at night.Although on both haze and non-haze days GOM showed rapid increase just before sunrise, they exhibited different trends during daytime from 10:00 to 18:00. On haze days, GOM

peaked in the afternoon when GEM was the lowest; the duration of the afternoon GOM peak was also longer on haze days.

4. Discussion

4.1 Influence of atmospheric mercury emission source

With the year-long data seasonal mercury emission sources couldbe inferred from the PSCF analysis. Fig.4a showed the overall spatial contribution of mercury emission sources in China. As Hefei is located in east-central China, its atmospheric mercury concentration could be affected by both north and south emission sources, including those from the North China Plain (especially Shandong Provice) and the neighboring provinces of Henan, Jiangsu, Jiangxi and Hubei. The total mercury emissions from Henan and Shandong provinces were estimated to be over 50 and 45 tons in 2010, respectively, making them two largest Hg emitters in China (Zhang et al., 2015b). Long-range transport could also impact seasonal variations of atmospheric mercury in Hefei. As shown in Fig.4, in spring, the major contributors of atmospheric mercury to Hefei were from the southwestern region including the local area and Jiangxi and Hunan Provinces. In summer, the main contributors were from north of Anhui, as well as Henan and Jiangxi Provinces, and even from the Pearl River Delta region in the far south. Since the number of haze daysaccountsonly for 5.6% of the total daysin spring and summer, we did not provide haze and non-haze PSCF results for spring and summer seasons. Asautumn and winter are the prevalent seasons for haze pollution, one PSCF result for haze days and another for non-haze days are shown forautumn and winter, respectively. The statistically significant difference ($p<0.001$) in the GEM concentration between non-haze days and haze days suggests that haze pollution

312 could directly affect the concentration of elemental mercury. As shown in Figs. 4d and
313 4f, higher GEM concentration was mainly influenced by local emission sources
314 onhaze days. Onnon-haze days, the most important mercury sources to the monitoring
315 site were not only the local emission sources, but also those from the neighboring
316 region of Shandong, Henan and Jiangxi Provinces (see Figs. 4e and 4g).Therefore, the
317 increase inthe GEM concentration on haze days was mainly caused by local
318 emissions.

319 GEM and CO often share similar anthropogenic emission sources, such as
320 industrial coal combustion, domestic coal combustion, iron and steel production and
321 cement production(Wu et al., 2006;Wang et al., 2005). However, they also have their
322 distinct emission sources. For instance, power plants and nonferrous metal smelters
323 emit mercury but hardly any CO; while automobiles contribute greatly to CO
324 emission, they are not a major emitter for mercury. The correlation coefficients and
325 slopes between GEM and CO concentrations during mercury pollution events are
326 shown in Table 3. These mercury pollution episodes were defined as when the hourly
327 average GEM concentration was higher than seasonal average GEM concentration for
328 at least 10 consecutive hours. These episodes could be classified into long-range
329 transport episodes or local episode by using the coefficients of determination (R^2) of
330 linear regression between Hg and CO: a significant positive correlation indicates
331 long-range transport episodes and a poor correlation signals local episodes(Jaffe et al.,
332 2005;Weiss-Penzias et al., 2006;Kim et al., 2009). Using this approach, we identified
333 three local episodes (events: 1-3) characterized by poor correlations between GEM
334 and CO concentrations (R^2:0.23-0.29),and four long-range transport episodes (events:
335 4-7) characterized by positive correlations between GEM and CO concentrations

(R^2:0.51-0.79).These local episodes tend to occur in autumn and winter. The slope of the trend line represents the Hg/CO ratio, which could aid in the identification of specific emission sources. Emissions from power plants typically have a higher Hg/CO ratio (Wu et al., 2006), whereas residential coal and biomass burning combustion have a lower Hg/CO ratio(0.0013-0.0046 ng m^{-3} $ppbv^{-1}$)due to incomplete combustion(Weiss-Penzias et al., 2007). The Hg/CO ratio for vehicles is close to zero (Zhang et al., 2013). The Hg/CO ratios during the pollution episodes in our study ranged from 0.0001 to 0.005ng m^{-3} $ppbv^{-1}$ suggesting mercury emission in autumn and winter in Hefei could be related to local incomplete combustion sources, such as residential coal and biomass burning.

4.2 Impacts of meteorological factors for atmospheric mercury on haze days

Meteorological conditions, especially wind direction and speed, could also impact atmospheric mercury on haze days. The wind rose for the monitoring site during the study period is shown in Fig.5. Easterly and southeasterly winds represented the prevailing wind directions at the study site. A wind rose diagram of GEM concentrations above the 90^{th} percentile value is shown in Fig.5B. We found that 67% of the high GEM concentrations occurred at low wind speed (below 1.5 m s^{-1}); however, wind speed below 1.5 m s^{-1} accounted for only 1.7% of the study duration. High GOM and PBM concentrations appear not to be related to high wind speed (wind speed: 3-5 m s^{-1}); only 1.4% and 2.6% of the high GOM and PBM concentrations were observed under high wind-speed conditions, respectively (Figs. 5C and 5D). The occurrence of high atmospheric mercury levels under low wind speed conditions is to be expected, as this slow wind speed condition is not

conductive to the spread and mixing of mercury especially on haze days, and thus favors mercury accumulation in the air. This further supports that atmospheric mercury on haze days is mainly due to by local emissions.

Both GEM and PBM concentrations exhibited diurnal variations with elevated concentrations at night or in early morning, regardless of the presence of haze. Such a diurnal variation could be related to changes in the height of the urban boundary layer. The diurnal trend of the boundary layer height (BLH or BLK) in Hefei is shown in Fig. S3, which is typically low in the morning and night, and high during the daytime on both non-haze and haze days. Such diurnal changes in BLH in Hefei and nearby cities have also been observed in previous studies(Yuan et al., 2005;Mao et al., 2006). The maximum PBM concentration (observed at 6:00) was more than 4 times higher than the minimum value (observed at 16:00) on both non-haze and haze days, with a 76% decrease from early morning to the afternoon. However, the reductions of PBM as a result of deposition during haze days was 62.7 pg m^{-3}, which was about 2.4 times that in non-haze days, suggesting that haze pollution could increase the removal of PBM. Although PBM is not the major form of atmospheric mercury, it is crucial in atmospheric mercury transport and removal processes due to its short atmospheric lifetime. As shown in Fig. 6, the highest PBM and $PM_{2.5}$ concentrations were observed in January, which is most likely dueto a shallower boundary layer in January than in other months. The co-variation in February is weaker, possibly due to the loss of PBM data because of instrument maintenance. The PBM concentration co-varied with the $PM_{2.5}$ concentration, especially in January when all the four PBM peak events were associated with increased $PM_{2.5}$ concentrations (Fig.6c). These results suggest that$PM_{2.5}$may play an important role in the formation of PBM. Thus, elevated PBM

concentrations in autumn and winter might be due to the combination of poor mixing conditions and higher PM concentrations.

4.3 Enhancement in GOM and the potential GEM oxidation mechanism

Diurnal variations of GEM, GOM, O_3 and CO concentrations on non-haze and haze days are shown in Fig. 7. The weak correlation (r=0.164) between GOM and CO suggests that theCO-producing, primary emission is not a major source of GOM in the air. This is clearly shown in Fig. 7 (haze days), where the peak value of GOM coincided with the lowest value of CO. As mentioned earlier, on both non-haze and haze days, GOM concentrations remained relatively constant during night, but increased rapidly prior to sunrise. However, GOM showed different trends during daytime (10:00-18:00) between non-haze and haze days. On non-haze days, a synchronous decline was found between GEM and GOM in the afternoon, but opposite trend was observed between GEM and GOM on haze days. This difference indicates that different GOM formation mechanisms might be at work on non-haze and haze days. Two processes can affect the GOM concentrations in the boundary layer air. The first is the change in the atmospheric boundary layer height, which could change the transport of GOM-enriched free tropospheric air. Secondly, in situ photochemical oxidation of GEM would increase the GOM concentration during daytime. Various atmospheric oxidants are capable of oxidizing GEM to GOM, including halogen radicals, ozone, hydroxyl radicals (OH), among others (Holmes et al., 2010;Wang et al., 2014).

It is well established that FT contains higher GOM concentrations than in the boundary layer(e.g.,(Murphy et al., 2006;Lyman and Jaffe, 2012;Timonen et al.,

2013;Brooks et al., 2014;Shah et al., 2016)).On both non-haze and haze days,it is thus possible that the higher GOM concentrations observed prior to sunrise aredue to enhanced admixingof the free tropospheric air as the boundary layer increases in the morning (see Fig. S3). On non-haze days, a synchronous decline in GEM and GOM throughout afternoon (10:00-18:00) might be related to the higher atmospheric boundary layer height during this period.However, on haze days, opposite variation was observed between GEM and GOM from 10:00-18:00, along with the elevated boundary layer height. This suggests that other than FT transport, photochemical oxidation of GEM might also play an important role in the enhancements of GOM. To determine the relative importance of FT transport and in situ photochemical oxidation, we examined the relationship between GOM and the changes in the height of the atmospheric boundary layer and the odd oxygen (O_X= O_3+NO_2)concentrations. We used O_x because it is a more conserved tracer of the extent of photochemical processes in the urban atmosphere (Herndon et al., 2008;Wood et al., 2010), as O_3 reacts with NO emitted from automobiles to form NO_2. Example results are shown in Fig. 8 for 20th November, 2013 (haze day). As can be seen from the figure, GEM and GOM showed opposite trends in the afternoon (12:00-16:00), along with higher $O_X$concentrationsduring this period.The height of the atmospheric boundary layer changed very little (less than 0.1 km) over the same period (see Fig. S4). This simple comparison suggests that the transport of FT GOM might be limited and that at least some of the GOM were formed from in situ oxidation of GEM. Note that in our studies we could only calculate daytime O_x concentrations, because NO_2 concentrations from MAX-DOAS were only available during daytime.

We further investiagted the mechanism of GEM oxidation to GOM. Ozone itself is not an efficient oxidant for GEM oxidation due to the low reaction rate (Hall, 1995;Holmes et al., 2010). Instead, halogen radicals (especially bromine atoms) and OH radicals, are believed to be the primary oxidants for GEM in the global troposphere (Holmes et al., 2010). Unfortunately, we did not measure halogen radicals in this study. OH radicals are known to be present in the early morning urban boundary layer, primarily from the photolysis of HONO, which accumulates duringnight (Kleffmann et al., 2005). Therefore, here we consider the oxdiation of GEM by OH radicals only. The formation of HgOH as an intermediate product of the Hg^0 (g) + OH oxidation reactions has been proposed bySommar et al., 2001, although HgOH is highly unstable and could decompose back rapidly to Hg^0 and OH (Sommar et al., 2001;Goodsite et al., 2004). It has been proposed that the presence of other gases X (X = NO_2, HO_2, RO, RO_2, orNO) could assist the formation of Hg(II) by formingX-HgOH,which outcompetesthe decomposition of HgOH(Calvert and Lindberg, 2005;Dibble et al., 2012;Wang et al., 2014). As an example, we calculated the transformation between GEM and GOM under the influence of NO_2, using the reactions and rate constants shown in Table S1. As shown in Fig. S5, the production rate of NO_2HgOH, d[NO_2HgOH]/dt, increasedalmost linearly with increasing NO_2 under low NO_2 concentrations, and eventually reached a steady state when the NO_2 concentration is high enough.

Based on the production rate of NO_2HgOH, we can estimate the production of NO_2HgOH during the 1hr sampling period when GOM was captured by the KCl-coated denuder in the Tekran 1130 unit.The production of NO_2HgOH and d[NO_2HgOH]/dt corresponding to different NO_2 concentrations is shown in Table 4.

With the increase of the NO_2 concentration, the contribution of the NO_2HgOH production to GOM will increase. If the NO_2 concentration is within 100 ppbv (from 0 to 100 ppbv), the production of NO_2HgOH would be in the range of 0.058-4.81 pg m^{-3} during the 1h sampling period. As illustrated in Table 4, the level of NO_2observed in our studyis high enough to account for the increase in the observed GOM production.Our results thus support a recent study in the tropical equatorial Pacific (Wang et al., 2014)that NO_2 aggregation with HgOH provides a possible mechanism for enhanced production of GOM. If that is true, NO_2 would be expected to play an even more important role in the urban air because of its higher concentration. More laboratory and modeling studies on the mercury oxidation mechanism in the presence of NO_2 and other gases are thus warranted.

5. Summary

Continuous measurements of speciated atmospheric mercury were conducted at Hefei, a mid-latitude inland city in central China, from July 2013 to June 2014. Measurements of other trace gases (e.g. CO, O_3, NO_2) and meteorological parameters were employed to better understand the sources and oxidation pathways of atmospheric mercury. The mean GEM, GOM and PBM concentrations during haze days were 4.74 ±1.62 ng m^{-3}, 4.32 ± 8.36 pg m^{-3} and 60.2 ± 131.4 pg m^{-3}, respectively. Potential source contribution function (PSCF) analysis suggested that the local mercury emission rather than long-range transport is the most important contributor of atmospheric mercury pollution on haze days at our monitoring site. The low GEM/CO ratio in Hefei could be indicative of local incomplete combustion sources such as residential coal and biomass burning. Haze pollution has a more profund impact on

PBM than on GEM and GOM. PBM showed a remarkable seasonal pattern, with higher concentrations in cold seasons and lower in warm seasons.Elevated PBM concentrations might be due to both the high loadings of particle matter and poorer mixing conditions on haze days especiallyin cold months.Both GEM and PBM concentrations exhibited great variations with elevated concentration during night.The diurnal variations of GEM and PBM might be related to the boundary layer depth; a lower boundary layer depth in the morning and night could elevate the mercury concentration.

Different from the diurnal variations of GEM and PBM, GOM concentration remained relatively constant at night, and then increased rapidly prior to the sunrise. The enhancement of GOM during daytime could be due to both the transport of GOM-enriched free troposphericair to the boundary layer and in situ oxidation of GEM in the boundary layer. Simple photochemical modeling supports the occurrence of daytime oxidation of GEM to GOM. Based on HgOH as an intermediate product, our calculations suggest that NO_2 aggregation with HgOH is a potential mechanism for the enhanced production of GOM in the inland urban air.

Acknowledgements

This research was supported by grants from the National Basic Research Program of China (2013CB430000), the National Natural Science Foundation of China (Project Nos. 91544103,41575021) and the External Cooperation Program of BIC, CAS (Project No.211134KYSB20130012).

References

Brooks, S., Luke, W., Cohen, M., Kelly, P., Lefer, B., and Rappenglück, B.: Mercury species measured atop the Moody Tower TRAMP site, Houston, Texas, Atmospheric Environment, 44, 4045-4055, 2010.

Brooks, S., Ren, X., Cohen, M., Luke, W. T., Kelley, P., Artz, R., Hynes, A., Landing, W., and Martos, B.: Airborne vertical profiling of mercury speciation near Tullahoma, TN, USA, Atmosphere, 5, 557-574, 2014.

Calvert, J. G., and Lindberg, S. E.: Mechanisms of mercury removal by O_3 and OH in the atmosphere, Atmospheric Environment, 39, 3355-3367, 2005.

Chen, L.-W. A., Chow, J. C., Doddridge, B. G., Dickerson, R. R., Ryan, W. F., and Mueller, P. K.: Analysis of a summertime $PM_{2.5}$ and haze episode in the mid-Atlantic region, Journal of the Air & Waste Management Association, 53, 946-956, 2003.

Cheng, I., Zhang, L., Mao, H., Blanchard, P., Tordon, R., and Dalziel, J.: Seasonal and diurnal patterns of speciated atmospheric mercury at a coastal-rural and a coastal-urban site, Atmospheric Environment, 82, 193-205, 2014.

Dibble, T., Zelie, M., and Mao, H.: Thermodynamics of reactions of ClHg and BrHg radicals with atmospherically abundant free radicals, Atmospheric Chemistry and Physics, 12, 10271-10279, 2012.

Draxler, R. R., and Hess, G.: An overview of the HYSPLIT_4 modelling system for trajectories, Australian meteorological magazine, 47, 295-308, 1998.

Duan, L., Xiu, G., Feng, L., Cheng, N., and Wang, C.: The mercury species and their association with carbonaceous compositions, bromine and iodine in $PM_{2.5}$ in Shanghai, Chemosphere, 146, 263-271, 2016.

527 Fang, F., Wang, Q., and Li, J.: Atmospheric particulate mercury concentration and its
528 dry deposition flux in Changchun City, China, Science of the total environment, 281,
529 229-236, 2001.
530 Fang, F., Wang, Q., and Li, J.: Urban environmental mercury in Changchun, a
531 metropolitan city in Northeastern China: source, cycle, and fate, Science of the Total
532 Environment, 330, 159-170, 2004.
533 Fang, G.-C., Wu, Y.-S., and Chang, T.-H.: Comparison of atmospheric mercury (Hg)
534 among Korea, Japan, China and Taiwan during 2000-2008, Journal of hazardous
535 materials, 162, 607-615, 2009.
536 Feng, X., Shang, L., Wang, S., Tang, S., and Zheng, W.: Temporal variation of total
537 gaseous mercury in the air of Guiyang, China, Journal of Geophysical Research:
538 Atmospheres (1984-2012), 109, 2004.
539 Friedli, H., Arellano Jr, A., Geng, F., Cai, C., and Pan, L.: Measurements of
540 atmospheric mercury in Shanghai during September 2009, Atmospheric Chemistry
541 and Physics, 11, 3781-3788, 2011.
542 Fu, X., Feng, X., Zhu, W., Wang, S., and Lu, J.: Total gaseous mercury concentrations
543 in ambient air in the eastern slope of Mt. Gongga, South-Eastern fringe of the
544 Tibetan plateau, China, Atmospheric Environment, 42, 970-979, 2008a.
545 Fu, X., Feng, X., Zhu, W., Zheng, W., Wang, S., and Lu, J. Y.: Total particulate and
546 reactive gaseous mercury in ambient air on the eastern slope of the Mt. Gongga area,
547 China, Applied Geochemistry, 23, 408-418, 2008b.
548 Fu, X., Feng, X., Qiu, G., Shang, L., and Zhang, H.: Speciated atmospheric mercury
549 and its potential source in Guiyang, China, Atmospheric Environment, 45,
550 4205-4212, 2011.

551 Fu, X., Feng, X., Liang, P., Zhang, H., Ji, J., and Liu, P.: Temporal trend and sources of
552 speciated atmospheric mercury at Waliguan GAW station, Northwestern China,
553 Atmospheric Chemistry and Physics, 12, 1951-1964, 2012.
554 Goodsite, M. E., Plane, J., and Skov, H.: A theoretical study of the oxidation of Hg^0 to
555 $HgBr_2$ in the troposphere, Environmental science & technology, 38, 1772-1776,
556 2004.
557 Gustin, M., and Jaffe, D.: Reducing the uncertainty in measurement and understanding
558 of mercury in the atmosphere, Environmental science & technology, 44, 2222-2227,
559 2010.
560 Gustin, M., Amos, H., Huang, J., Miller, M., and Heidecorn, K.: Measuring and
561 modeling mercury in the atmosphere: a critical review, Atmospheric Chemistry and
562 Physics, 15, 5697-5713, 2015.
563 Gustin, M. S., Huang, J., Miller, M. B., Peterson, C., Jaffe, D. A., Ambrose, J., Finley, B.
564 D., Lyman, S. N., Call, K., and Talbot, R.: Do we understand what the mercury
565 speciation instruments are actually measuring? Results of RAMIX, Environmental
566 science & technology, 47, 7295-7306, 2013.
567 Hall, B.: The gas phase oxidation of elemental mercury by ozone, in: Mercury as a
568 Global Pollutant, Springer, 301-315, 1995.
569 Herndon, S. C., Onasch, T. B., Wood, E. C., Kroll, J. H., Canagaratna, M. R., Jayne, J.
570 T., Zavala, M. A., Knighton, W. B., Mazzoleni, C., and Dubey, M. K.: Correlation of
571 secondary organic aerosol with odd oxygen in Mexico City, Geophysical Research
572 Letters, 35, 2008.

573 Holmes, C. D., Jacob, D. J., Corbitt, E. S., Mao, J., Yang, X., Talbot, R., and Slemr, F.:
574 Global atmospheric model for mercury including oxidation by bromine atoms,
575 Atmospheric Chemistry and Physics, 10, 12037-12057, 2010.
576 Hu, Q. H., Kang, H., Li, Z., Wang, Y. S., Ye, P. P., Zhang, L. L., Yu, J., Yu, X. W., Sun,
577 C., and Xie, Z. Q.: Characterization of atmospheric mercury at a suburban site of
578 central China from wintertime to springtime, Atmospheric Pollution Research, 5,
579 769-778, 2014.
580 Huang, J., Miller, M. B., Weiss-Penzias, P., and Gustin, M. S.: Comparison of gaseous
581 oxidized Hg measured by KCl-coated denuders, and nylon and cation exchange
582 membranes, Environmental science & technology, 47, 7307-7316, 2013.
583 Jaffe, D., Prestbo, E., Swartzendruber, P., Weiss-Penzias, P., Kato, S., Takami, A.,
584 Hatakeyama, S., and Kajii, Y.: Export of atmospheric mercury from Asia,
585 Atmospheric Environment, 39, 3029-3038, 2005.
586 Kim, S.-H., Han, Y.-J., Holsen, T. M., and Yi, S.-M.: Characteristics of atmospheric
587 speciated mercury concentrations (TGM, Hg (II) and Hg (p)) in Seoul, Korea,
588 Atmospheric Environment, 43, 3267-3274, 2009.
589 Kleffmann, J., Gavriloaiei, T., Hofzumahaus, A., Holland, F., Koppmann, R., Rupp, L.,
590 Schlosser, E., Siese, M., and Wahner, A.: Daytime formation of nitrous acid: A
591 major source of OH radicals in a forest, Geophysical Research Letters, 32, 2005.
592 Landis, M. S., Stevens, R. K., Schaedlich, F., and Prestbo, E. M.: Development and
593 characterization of an annular denuder methodology for the measurement of
594 divalent inorganic reactive gaseous mercury in ambient air, Environmental science
595 & technology, 36, 3000-3009, 2002.

596 Li, J., Sommar, J., Wängberg, I., Lindqvist, O., and Wei, S.-q.: Short-time variation of
597 mercury speciation in the urban of Göteborg during GÖTE-2005, Atmospheric
598 Environment, 42, 8382-8388, 2008.
599 Lindberg, S., Bullock, R., Ebinghaus, R., Engstrom, D., Feng, X., Fitzgerald, W.,
600 Pirrone, N., Prestbo, E., and Seigneur, C.: A synthesis of progress and uncertainties
601 in attributing the sources of mercury in deposition, AMBIO: A Journal of the
602 Human Environment, 36, 19-33, 2007.
603 Lindqvist, O., and Rodhe, H.: Atmospheric mercury-a review*, Tellus B, 37, 1985.
604 Liu, B., Keeler, G. J., Dvonch, J. T., Barres, J. A., Lynam, M. M., Marsik, F. J., and
605 Morgan, J. T.: Urban-rural differences in atmospheric mercury speciation,
606 Atmospheric Environment, 44, 2013-2023, 2010.
607 Lyman, S. N., and Jaffe, D. A.: Formation and fate of oxidized mercury in the upper
608 troposphere and lower stratosphere, Nature Geoscience, 5, 114-117, 2012.
609 Mao, M., Jiang, W., Wu, X., Qi, F., Yuan, R., Fang, H., Liu, D., and Zhou, J.: LIDAR
610 exploring of the UBL in downtown of the Nanjing City, Acta Scientiae
611 Circumstantiae, 26, 1723-1728, 2006.
612 Marumoto, K., Hayashi, M., and Takami, A.: Atmospheric mercury concentrations at
613 two sites in the Kyushu Islands, Japan, and evidence of long-range transport from
614 East Asia, Atmospheric Environment, 117, 147-155, 2015.
615 Murphy, D., Hudson, P., Thomson, D., Sheridan, P., and Wilson, J.: Observations of
616 mercury-containing aerosols, Environmental science & technology, 40, 3163-3167,
617 2006.

618 Pacyna, E. G., Pacyna, J. M., Steenhuisen, F., and Wilson, S.: Global anthropogenic
619 mercury emission inventory for 2000, Atmospheric environment, 40, 4048-4063,
620 2006.
621 Pacyna, E. G., Pacyna, J., Sundseth, K., Munthe, J., Kindbom, K., Wilson, S.,
622 Steenhuisen, F., and Maxson, P.: Global emission of mercury to the atmosphere
623 from anthropogenic sources in 2005 and projections to 2020, Atmospheric
624 Environment, 44, 2487-2499, 2010.
625 Peterson, C., Alishahi, M., and Gustin, M. S.: Testing the use of passive sampling
626 systems for understanding air mercury concentrations and dry deposition across
627 Florida, USA, Science of the Total Environment, 424, 297-307, 2012.
628 Polissar, A. V., Hopke, P. K., and Harris, J. M.: Source regions for atmospheric aerosol
629 measured at Barrow, Alaska, Environmental science & technology, 35, 4214-4226,
630 2001.
631 Ren, X., Luke, W. T., Kelley, P., Cohen, M. D., Artz, R., Olson, M. L., Schmeltz, D.,
632 Goldberg, D. L., Ring, A., and Mazzuca, G. M.: Atmospheric mercury
633 measurements at a suburban site in the Mid-Atlantic United States: Inter-annual,
634 seasonal and diurnal variations and source-receptor relationships, Atmospheric
635 Environment, 2016.
636 Schroeder, W. H., and Munthe, J.: Atmospheric mercury-an overview, Atmospheric
637 Environment, 32, 809-822, 1998.
638 Shah, V., Jaeglé, L., Gratz, L., Ambrose, J., Jaffe, D., Selin, N., Song, S., Campos, T.,
639 Flocke, F., and Reeves, M.: Origin of oxidized mercury in the summertime free
640 troposphere over the southeastern US, Atmospheric Chemistry and Physics, 16,
641 1511-1530, 2016.

642 Sommar, J., Gårdfeldt, K., Strömberg, D., and Feng, X.: A kinetic study of the
643 gas-phase reaction between the hydroxyl radical and atomic mercury, Atmospheric
644 Environment, 35, 3049-3054, 2001.
645 Streets, D. G., Hao, J., Wu, Y., Jiang, J., Chan, M., Tian, H., and Feng, X.:
646 Anthropogenic mercury emissions in China, Atmospheric Environment, 39,
647 7789-7806, 2005.
648 Sun, Z., Mu, Y., Liu, Y., and Shao, L.: A comparison study on airborne particles during
649 haze days and non-haze days in Beijing, Science of the total environment, 456, 1-8,
650 2013.
651 Timonen, H., Ambrose, J., and Jaffe, D.: Oxidation of elemental Hg in anthropogenic
652 and marine airmasses, Atmospheric Chemistry and Physics, 13, 2827-2836, 2013.
653 Wan, Q., Feng, X., Lu, J., Zheng, W., Song, X., Han, S., and Xu, H.: Atmospheric
654 mercury in Changbai Mountain area, northeastern China I. The seasonal distribution
655 pattern of total gaseous mercury and its potential sources, Environmental research,
656 109, 201-206, 2009a.
657 Wan, Q., Feng, X., Lu, J., Zheng, W., Song, X., Li, P., Han, S., and Xu, H.: Atmospheric
658 mercury in Changbai Mountain area, northeastern China II. The distribution of
659 reactive gaseous mercury and particulate mercury and mercury deposition fluxes,
660 Environmental research, 109, 721-727, 2009b.
661 Wang, F., Saiz-Lopez, A., Mahajan, A., Martín, J. G., Armstrong, D., Lemes, M., Hay,
662 T., and Prados-Roman, C.: Enhanced production of oxidised mercury over the
663 tropical Pacific Ocean: a key missing oxidation pathway, Atmospheric Chemistry
664 and Physics, 14, 1323, 2014.

Wang, L., Zhang, Q., Hao, J., and He, K.: Anthropogenic CO emission inventory of Mainland China, Acta Scientiae Circumstantiae, 25, 1580-1585, 2005.

Wang, Y., Zhang, X., and Draxler, R. R.: TrajStat: GIS-based software that uses various trajectory statistical analysis methods to identify potential sources from long-term air pollution measurement data, Environmental Modelling & Software, 24, 938-939, 2009.

Weigelt, A., Temme, C., Bieber, E., Schwerin, A., Schuetze, M., Ebinghaus, R., and Kock, H. H.: Measurements of atmospheric mercury species at a German rural background site from 2009 to 2011–methods and results, Environmental Chemistry, 10, 102-110, 2013.

Weiss-Penzias, P., Jaffe, D. A., Swartzendruber, P., Dennison, J. B., Chand, D., Hafner, W., and Prestbo, E.: Observations of Asian air pollution in the free troposphere at Mount Bachelor Observatory during the spring of 2004, Journal of Geophysical Research: Atmospheres, 111, 2006.

Weiss-Penzias, P., Jaffe, D., Swartzendruber, P., Hafner, W., Chand, D., and Prestbo, E.: Quantifying Asian and biomass burning sources of mercury using the Hg/CO ratio in pollution plumes observed at the Mount Bachelor Observatory, Atmospheric Environment, 41, 4366-4379, 2007.

Wood, E., Canagaratna, M., Herndon, S., Onasch, T., Kolb, C., Worsnop, D., Kroll, J., Knighton, W., Seila, R., and Zavala, M.: Investigation of the correlation between odd oxygen and secondary organic aerosol in Mexico City and Houston, Atmospheric Chemistry and Physics, 10, 8947-8968, 2010.

687 Wu, Y., Wang, S., Streets, D. G., Hao, J., Chan, M., and Jiang, J.: Trends in
688 anthropogenic mercury emissions in China from 1995 to 2003, Environmental
689 science & technology, 40, 5312-5318, 2006.
690 Xu, X., and Akhtar, U.: Identification of potential regional sources of atmospheric total
691 gaseous mercury in Windsor, Ontario, Canada using hybrid receptor modeling,
692 Atmospheric Chemistry and Physics, 10, 7073-7083, 2010.
693 Yuan, S., Xin, Y., and Zhou, J.: Lidar Observations of the Lower Atmosphere in Hefei,
694 Chinese Journal of Atmospheric Sciences, 29, 387-395, 2005.
695 Zhang, H., Fu, X., Lin, C., Wang, X., and Feng, X.: Observation and analysis of
696 speciated atmospheric mercury in Shangri-La, Tibetan Plateau, China, Atmospheric
697 Chemistry and Physics, 15, 653-665, 2015a.
698 Zhang, L., Wang, S., Wang, L., and Hao, J.: Atmospheric mercury concentration and
699 chemical speciation at a rural site in Beijing, China: implications of mercury
700 emission sources, Atmospheric Chemistry and Physics, 13, 10505-10516, 2013.
701 Zhang, L., Wang, S., Wang, L., Wu, Y., Duan, L., Wu, Q., Wang, F., Yang, M., Yang, H.,
702 and Hao, J.: Updated Emission Inventories for Speciated Atmospheric Mercury
703 from Anthropogenic Sources in China, Environmental science & technology, 49,
704 3185-3194, 2015b.
705
706

707 **Table 1. Summary of GEM, GOM and PBM concentrations measured in Hefei**

708 **from July 2013 to June 2014.**

709

	GEM (ng m^{-3})			GOM (pg m^{-3})			PBM (pg m^{-3})		
	Mean±σ	Range	N	Mean±σ	Range	N	Mean±σ	Range	N
Spring	3.89±1.79	0.2-21.3	7890	4.49±4.22	0.5-69.8	526	8.34±8.97	1.6-130.1	542
Summer	4.08±1.99	0.3-22.9	6050	3.66±4.39	0.5-45.2	511	3.61±4.38	0.5-41.9	570
Autumn	4.51±2.10	0.4-23.8	3632	5.65±8.93	0.5-78.9	274	59.9±153.5	0.5-1615	339
Winter	4.05±1.81	0.9-12.2	6381	2.59±2.58	0.5-9.5	541	56.1±134.9	0.5-1827	639
Total	4.07±1.91	0.2-23.8	23953	3.67±5.11	0.5-78.9	1852	30.02±100.3	0.5-1827	2090
Non-haze	3.95±1.93	0.2-23.8	20345	2.49±2.41	0.5-33.5	1508	23.3±90.76	0.5-1827	1708
Haze	4.74±1.62	2.1-16.5	3608	4.32±8.36	0.5-78.9	344	60.2±131.4	1.6-1615	382

710

711

712 **Table 2.Speciated atmospheric mercury concentrations in Hefei and other urban**

713 **and rural areas.**

714

Location	Classification	Time	TGM ($ng\ m^{-3}$)	GEM ($ng\ m^{-3}$)	GOM ($pg\ m^{-3}$)	PBM ($pg\ m^{-3}$)	Reference
Hefei	Suburb	Jul 2013-Jun 2014	4.1	4.07	3.67	30	This study
Hefei	Suburb	Feb-May 2009	2.53	-	-	-	Hu et al. (2014)
Beijing	Rural	Dec2008-Nov2009	3.23	3.22	10.1	98.2	Zhang et al. (2013)
Shanghai	Urban	Aug-Sep 2009	2.7	-	-	-	Friedli et al. (2011)
Nanjing	Urban	Jan-Dec 2011	7.9	-	-	-	Zhu et al. (2012)
Guiyang	Urban	Nov 2001-Nov 2002	8.4	-	-	-	Fenget al. (2004)
Guiyang	Urban	Aug-Dec 2009	-	9.72	35.7	368	Fu et al. (2011)
Changchun	Urban	Jul 1999-Jan 2000	18.4	-	-	276	Fang et al. (2004)
Changchun	Suburb	Jul 1999-Jan 2000	11.7	-	-	109	Fang et al. (2004)
Mt.Changbai	Remote	Aug2005-Jul 2006	3.58	-	65	77	Wan et al. (2009a,b)
Mt.Gongga	Remote	May 2005-July 2006	3.98	-	6.2	30.7	Fu et al. (2008a,b)
Mt.Waliguan	Remote	Sep 2007-Aug 2008	1.98	-	7.4	19.4	Fu et al. (2012a)
Mt.Leigong	Remote	May2008-May 2009	2.8	-	-	-	Fu et al. (2010)
Shangri-La	Remote	Nov 2009-Nov 2010	2.55	-	8.22	38.82	Zhang (2015)
Detroit, USA	Urban	Jan-Dec 2004	-	2.5	15.5	18.1	Liu et al. (2010)
Dexter, USA	Rural	Jan-Dec 2004	-	1.6	3.8	6.1	Liu et al. (2010)
Houston, USA	Urban	Aug-Oct 2006	-	1.66	6.9	2.5	Brooks et al. (2010)
Florida, USA	Urban	Jul 2009-Jul 2010		1.3	3	2	Peterson et al. (2012)
Maryland, USA	suburb	2007-2015		1.41	4.6	8.6	Ren et al. (2016)
Göteborg,Sweden	Urban	Feb-Mar 2005	-	1.96	2.53	12.5	Li et al. (2008)
Nova Scotia,Canada	Urban	Jan 2010- Dec 2011		1.67	2.07	2.32	Cheng et al.(2014)
Northern Hemisphere background value					1.5-1.7		Lindberg et al. (2007)

715

716 **Table 3. Coefficients of determination and slopes between GEM and CO**

717 **concentrationsduring atmospheric mercury pollution episodes (*p<0.01).**

718

Event	Start Time (UTC + 8 hr)	End Time (UTC + 8 hr)	Duration (h)	GEM (ng m^{-3})	CO (ppbv)	GEM/CO (slope, ng m^{-3} $ppbv^{-1}$)	R^2
1	2013/11/21 03:00	2013/11/22 02:00	23	8.37±2.42	4481.6±717.3	0.0018	0.29*
2	2013/12/07 04:00	2013/12/09 04:00	48	9.21±1.16	5943.8±1394.1	0.0004	0.23*
3	2014/01/17 22:00	2014/01/19 13:00	39	5.80±0.83	5746.3±1626.9	0.0003	0.28*
4	2014/01/25 02:00	2014/01/25 22:00	20	6.03±0.50	8797.9±2244.3	0.0002	0.59*
5	2014/03/16 05:00	2014/03/16 20:00	15	4.46±0.47	2261.7±440.2	0.0010	0.79*
6	2014/03/17 06:00	2014/03/18 12:00	30	8.85±2.46	2697.1±590.3	0.0030	0.51*
7	2014/05/21 00:00	2014/05/21 11:00	11	5.74±0.94	3676.7±1690.0	0.0050	0.79*

719 Notes: these episodes were identified when the hourly average GEM concentration

720 was higher than the seasonal average GEM concentration for more than 10

721 consecutive hours

722

723

724 **Table 4.The production of NO_2HgOH and d[NO_2HgOH]/dtat different NO_2**

725 **concentrations**

NO2 (ppbv)	10	20	30	40	50	60	70	80	90	100
d(NO_2HgOH)/dt (molecule cm^{-3} s^{-1})	0.36	0.71	1.04	1.37	1.68	1.99	2.28	2.56	2.83	3.10
NO2HgOH (pg m^{-3}, 1hr)	0.56	1.10	1.63	2.13	2.61	3.08	3.54	3.97	4.40	4.81

726

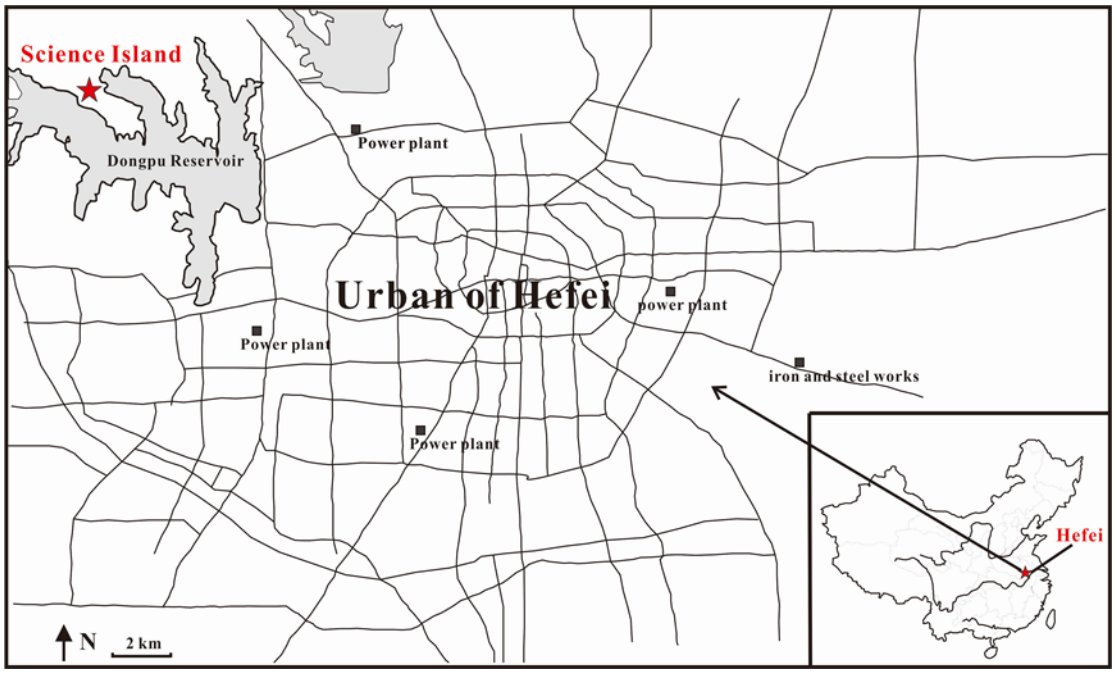

Fig. 1. Location of the study site in Hefei, China.

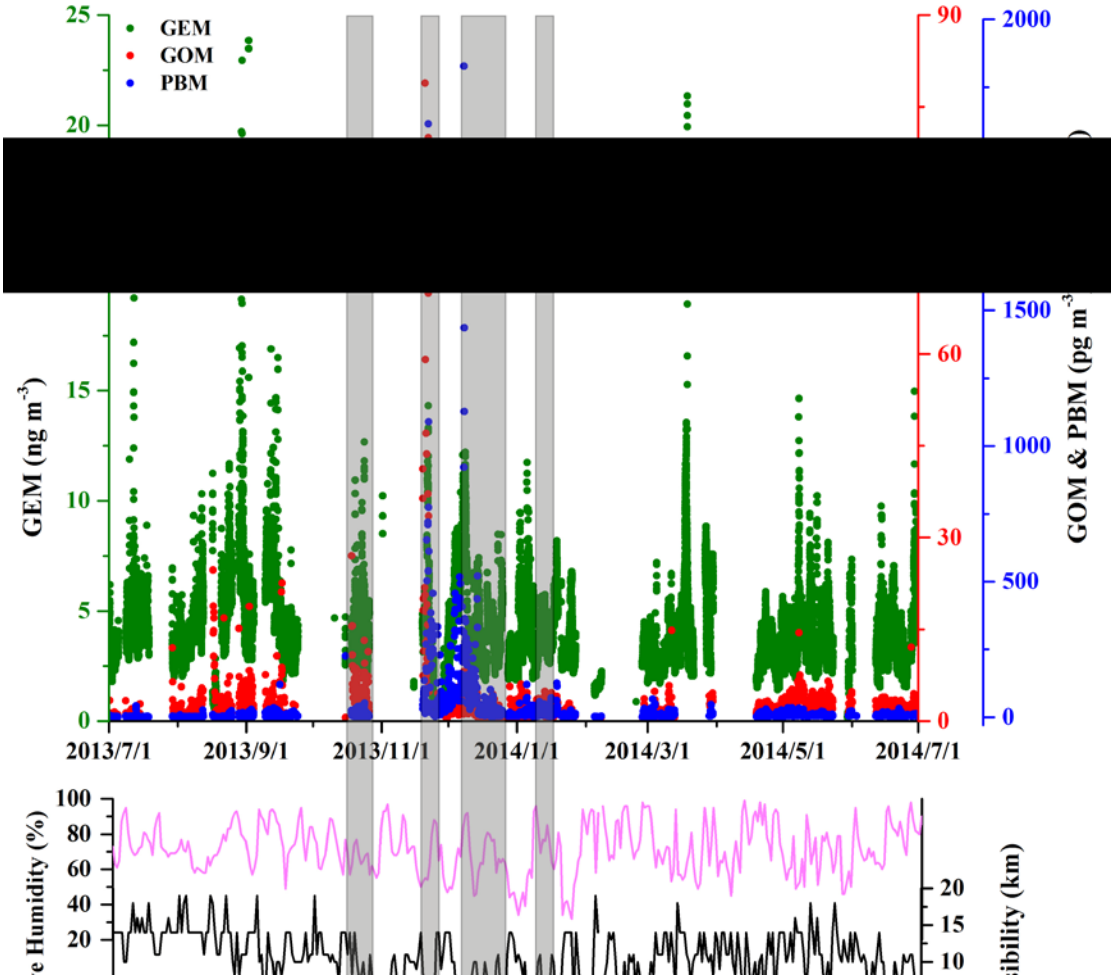

Fig. 2. Time series of GEM, GOM and PBM concentrations, along with visibility, relatively humidity, at the monitoring site in Hefei from July 2013 to June 2014. The GEM data were at a 5-min resolution, and the GOM and PBM data were two-hour averages. The gray columns show the major haze pollution episodes occurred during the study period.

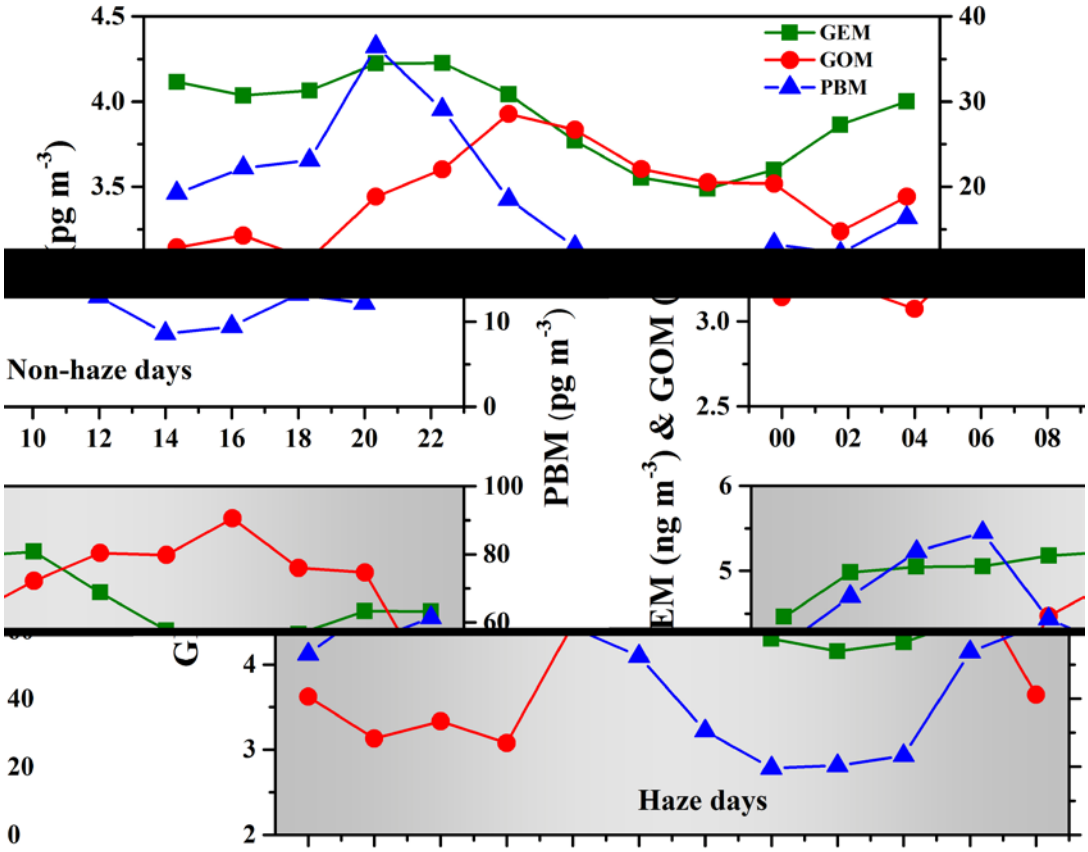

Fig. 3. Diurnal trends of GEM, GOM and PBM concentrations in Hefei on non-haze and haze days (Local time = UTC + 8 hr). The data were two-hour averages.

752

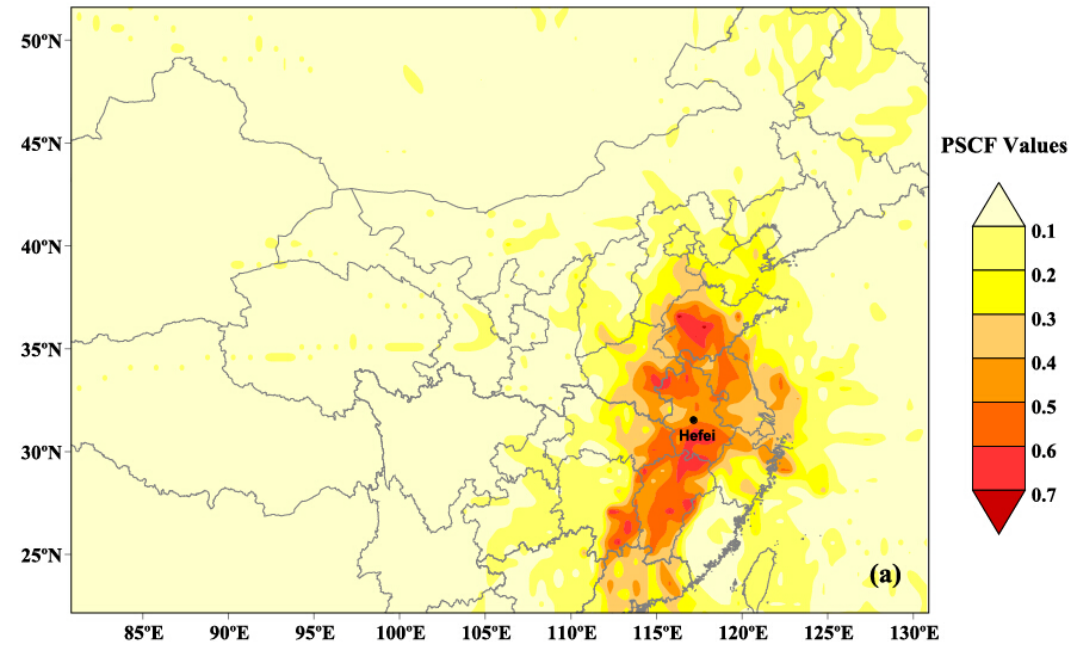

753

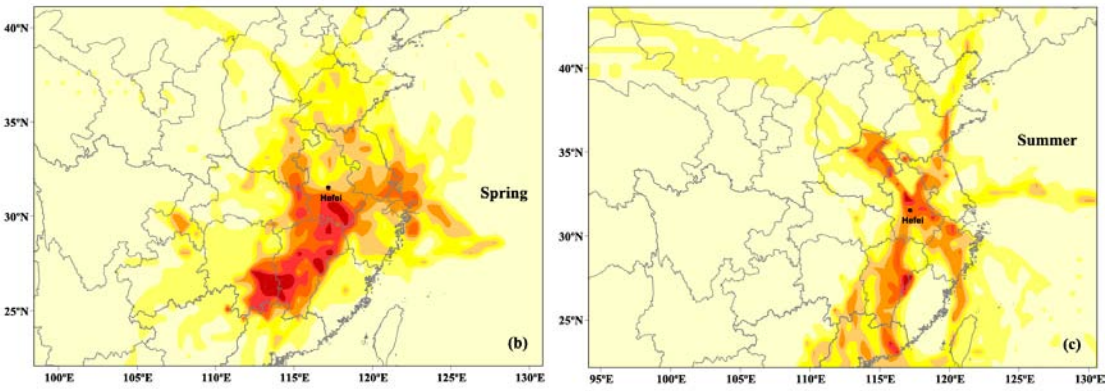

754

755

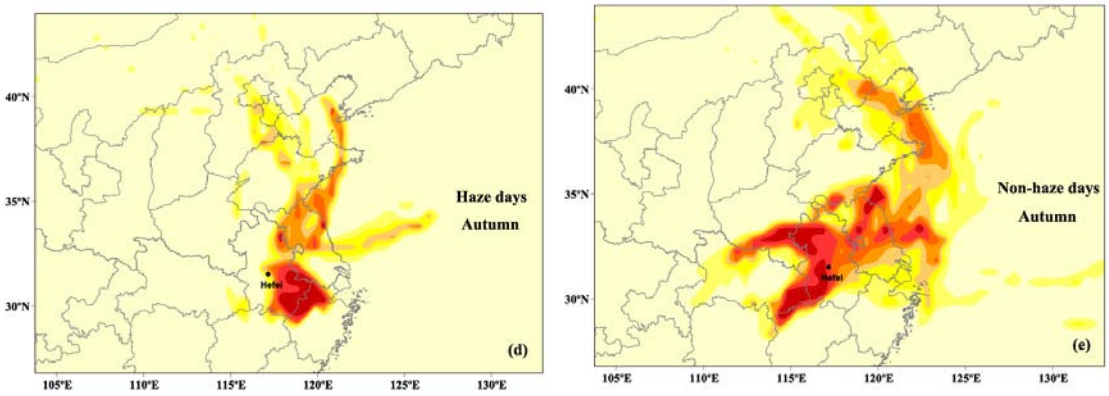

756

757

758

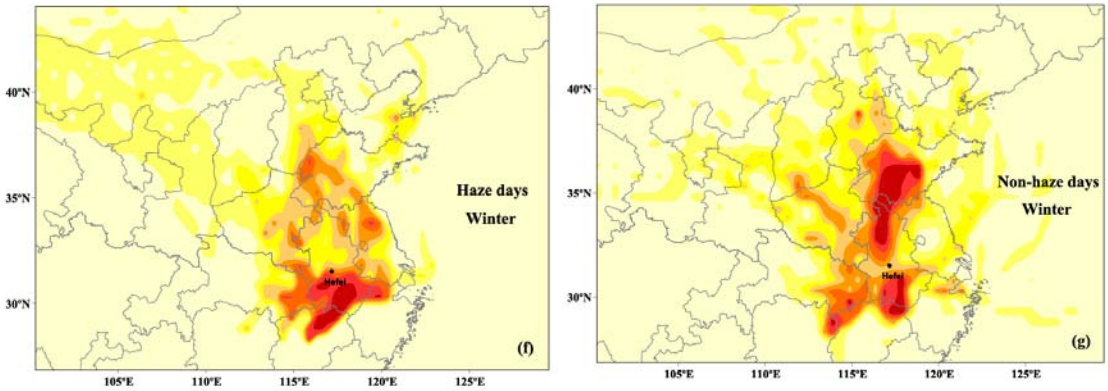

Fig. 4. Likely emission source areas of GEM identified by PSCF analysis. (a) overall (from July 2013 to June 2014), (b) spring, (c) summer, (d) haze days in autumn, (e) non-haze days in autumn, (f) haze days in winter, (g) non-haze days in winter.

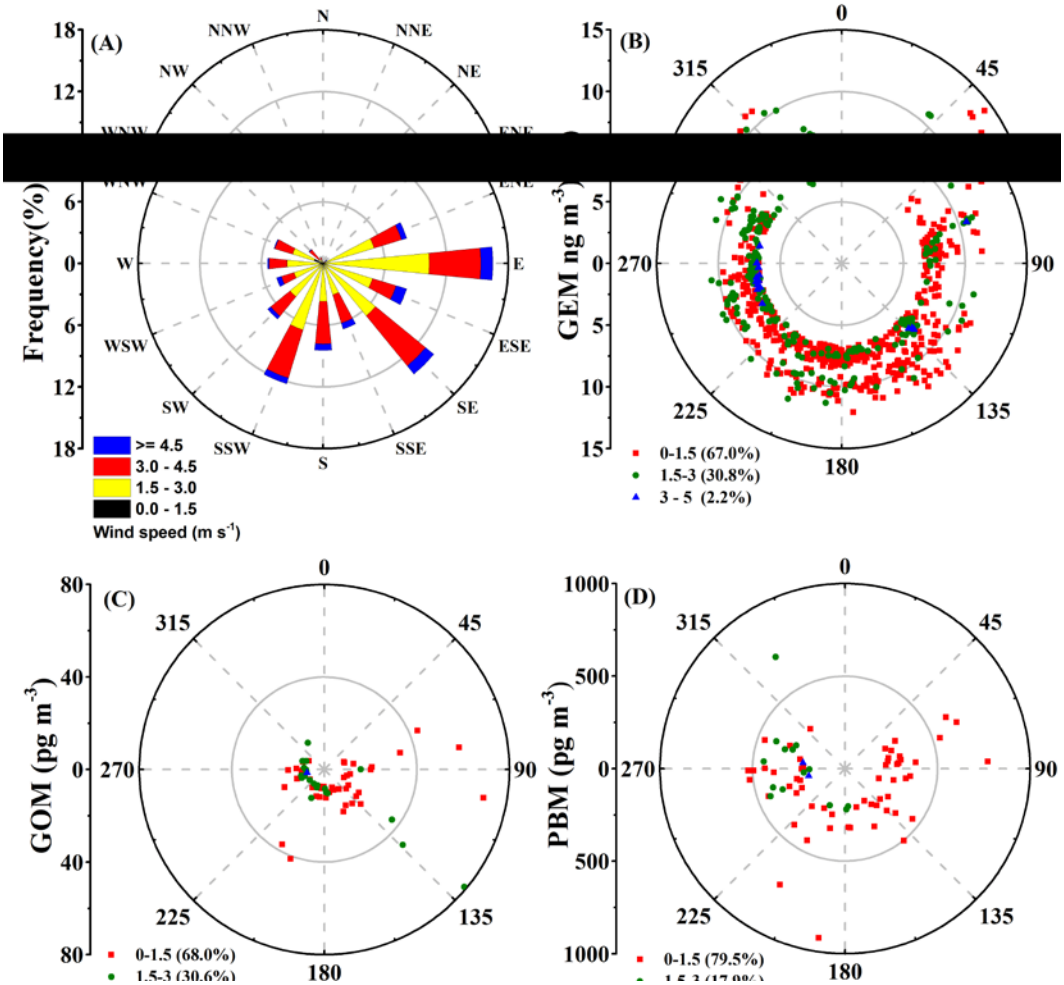

Fig. 5. Wind direction and speed at the monitoring station during the study period. (A) the wind rose for the entire study period; (B), (C) and (D) are the wind rose diagrams for GEM, GOM and PBM concentrations above the 90th percentile values, respectively.

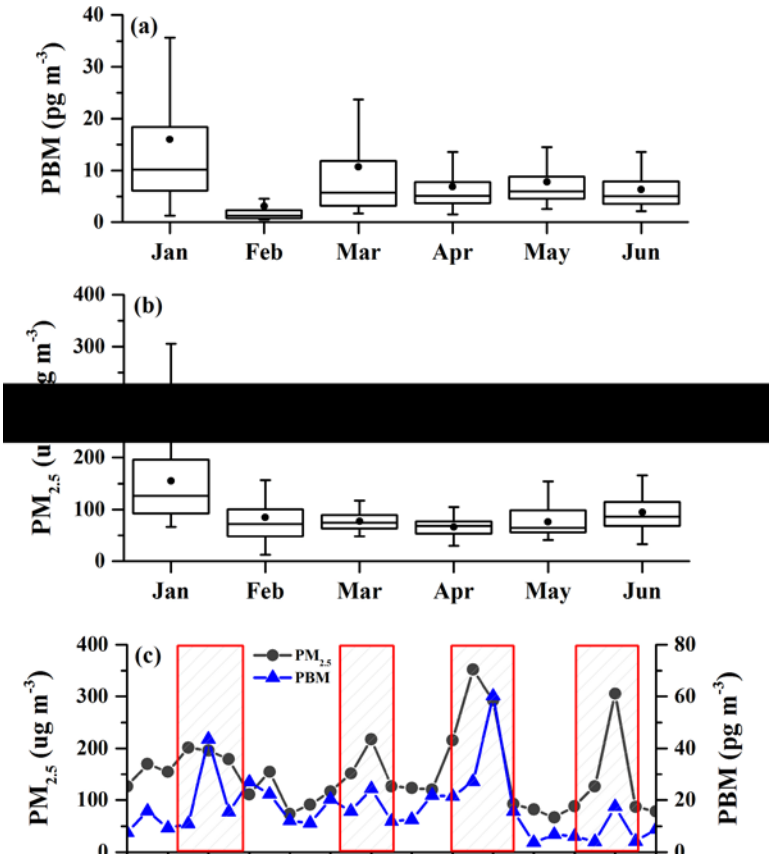

Fig. 6. Monthly variation of (a) PBM and (b) $PM_{2.5}$concentrations from January to June, 2014, (c) average daily $PM_{2.5}$ and PBM concentrations in January, 2014.

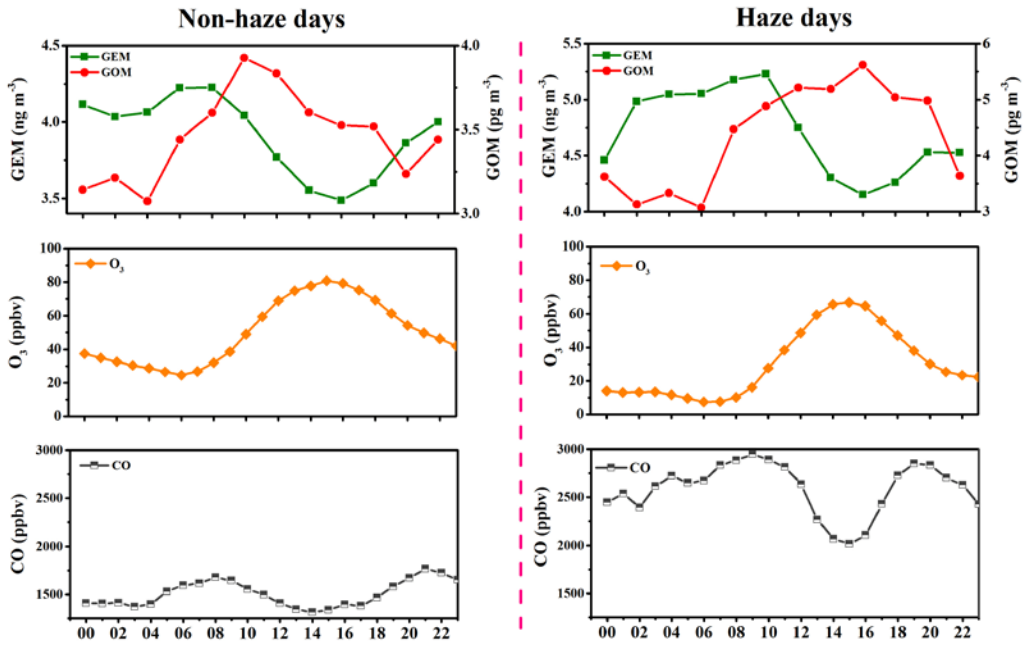

Fig. 7. Diurnal variations of GEM, GOM, $O_3$and COconcentrations on non-haze and haze days.

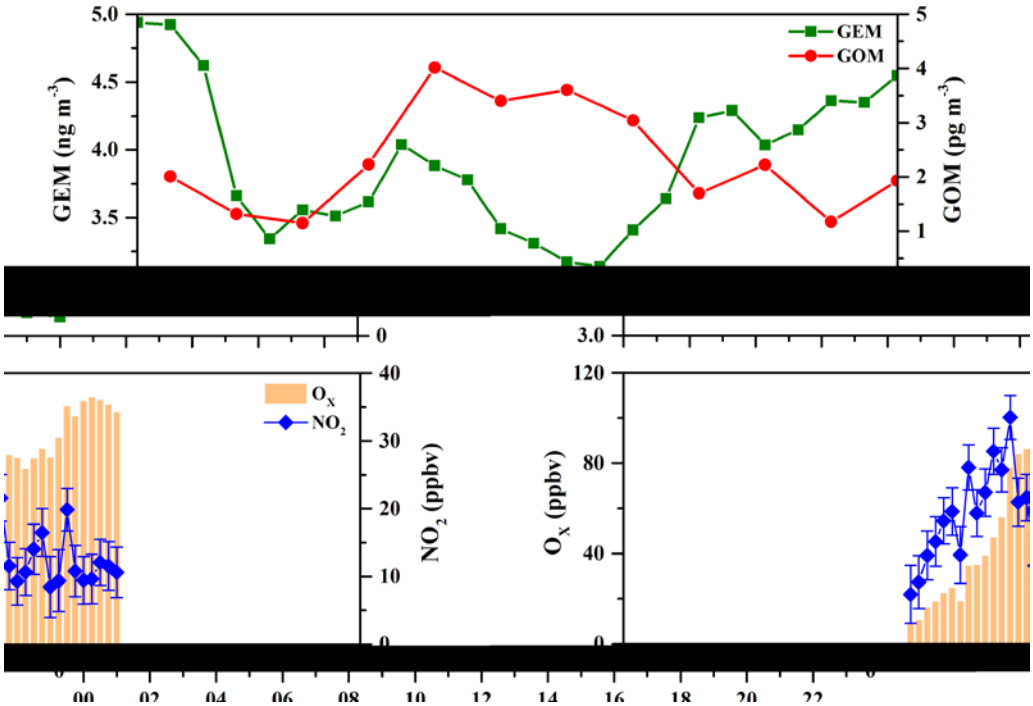

Fig. 8. A case study of diurnal variations of GEM, GOM, O_X,and NO_2at Hefei (20th November, 2013).The top panel shows the hourly averaged GEM and GOM concentrations, and the bottom panel shows the O_X (O_X= NO_2 +O_3) and the NO_2 concentrations. The error bars for NO_2 refer to the NO_2 standard errors.